Zn^{2+} Ions Selectively Induce Antimicrobial Salivary Peptide Histatin-5 To Fuse Negatively Charged Vesicles. Identification and Characterization of a Zinc-Binding Motif Present in the Functional Domain†

Sonia Melino,‡ Stefano Rufini,§ Marco Sette,§ Roberto Morero,|| Alessandro Grottesi,⊥ Maurizio Paci,§ and Raffaele Petruzzelli*,‡

Dipartimento di Scienze Biomediche, Università di Chieti "G. D'Annunzio", 66100 Chieti, Italy, Dipartmenti di "Biologia" e di "Scienze Chimiche e Tecnologiche", Università di Roma "Tor Vergata", Roma, Italy, Instituto de Quimica Biologica, Universidad Nacional de Tucumàn, San Miguel de Tucumàn, Argentina, and Dipartimento di Chimica, Università di Roma La Sapienza, Roma, Italy

Received January 27, 1999; Revised Manuscript Received May 19, 1999

ABSTRACT: The salivary antimicrobial peptide histatin-5 is able to aggregate and fuse negatively charged small unilamellar vesicles, and this fusogenic activity is selectively induced by the presence of zinc ions. Circular dichroism spectroscopy shows that histatin-5, in the presence of negatively charged vesicles and zinc ions, undergoes a conformational change leading to the stabilization of an α-helical secondary structure. We attribute the specific action of the zinc ions to the presence of a consensus sequence, HEXXH, located in the C-terminal functional domain of histatin-5, a recognized zinc-binding motif in many proteins. Two-dimensional proton NMR spectroscopy of histatin-5 in a trifluoroethanol/water mixture (a membrane mimetic environment) has been performed and the results analyzed by means of distance geometry and restrained molecular dynamics simulations. Our results reveal that the peptide chain, including the Zn-binding consensus sequence corresponding to residues 15−19, is in a helicoidal conformation. Comparison of the chemical shifts of the individual amino acids in histatin-5 with those recently reported in other solvents indicates that trifluoroethanol/water has a structuring capability somewhere between water and dimethyl sulfoxide. The mechanism of action of this antimicrobial peptide is discussed on the basis of its structural characteristics with particular attention to the Zn-binding motif.

Antimicrobial peptides are molecular effectors of the innate nonimmune defense system existing in all animals (*1, 2*). Human saliva is a source of numerous proteins and enzymes; in fact, the human parotid and the submandibular−sublingual glands are known to secrete many proteins and peptides that are electrophoretically distinguishable. Some of the salivary proteins for which the primary structure is known include the proline-rich proteins, such as the statherins, the cystatins (*3*), and the histidine-rich proteins (histatins) (*4, 5*).

The histatins are a family of related cationic histidine-rich polypeptides of variable length. The primary structure of the major family members (histatins-1, -3, and -5) has been determined and indicates that these peptides consist of 38, 32, and 24 amino acids, respectively (*6*). Many of the smaller members of the histatin family are proteolytic products of Hst1 and -3 (*6*−*8*).

The histatins have a noticeable efficiency in their antimicrobial activity and have been shown to exhibit a remarkable inhibitory effect at physiological concentrantion on the germination of *Candida albicans* (*5, 9*). Among the histatins, histatin-5 has been reported to be the most efficient in killing *C. albicans* (*6*). Raj et al. (*10*) demonstrated that the synthetic C-terminal 16-residue fragment of histatin-5 possesses the same candidacidal activity of the entire molecule and this activity has been correlated to the propensity of this fragment to assume, in a hydrophobic environment, a nonamphipathic α-helical structure. The mechanism of action of these peptides is still unknown, and specific receptors for histatins have not been yet identified, but the cationic nature of histatins suggests that their antimicrobial activity may be dependent upon electrostatic interactions rather than the ability to introduce pores in biological membranes, as found for other natural antimicrobial peptides (*11, 12*).

In this study, we demonstrate that histatin-5 is able to aggregate negatively charged vesicles, thus confirming that the electrostatic interactions play an essential role in the action of this peptide. Moreover, we demonstrate that histatin-5 is able to fuse negatively charged vesicles (SUVs)[1] only in the presence of Zn^{2+} ions.

This metal cofactor induces a conformational change in histatin-5 in the presence of negatively charged vesicles as revealed by circular dichroism spectroscopy. This conformational change can be correlated to the dimerization effect

† This work was supported by Contributo CNR no. 96.03712.CT14. The Strategic project of CNR "Structural Biology" and the MURST project "Strutture, Meccanismi ed Ingegneria di Proteine" are acknowledged. The CNR "Progetto Finalizzato Biotecnologie" is acknowledged for the execution of this work.

* Correspondence should be addressed to this author at the Dipartimento di Scienze Biomediche, Università "G. D'Annunzio", Via dei Vestini, 66100 Chieti, Italy. Telephone: +39 871 3555313. Fax: +39 871 3555356. Email: r.petruzzelli@dsb.unich.it.

‡ Università di Chieti "G. D'Annunzio".

§ Università di Roma "Tor Vergata".

|| Universidad Nacional de Tucumàn.

⊥ Università di Roma La Sapienza.

10.1021/bi990212c CCC: $18.00 © 1999 American Chemical Society
Published on Web 07/02/1999

induced by zinc. We have correlated the selective action of the zinc ions with the presence in the C-terminal region, the presumed functional domain of the histatins, of a structural motif [HisGluXXHis] found in Zn-proteases and Zn-binding toxins (*13*). This motif is conserved in all the major human histatins and in the histatins isolated from the subhuman primate *Macaca fascicularis* (*14*). The solution structure of histatin-5 in TFE/water mixtures, as determined by NMR spectroscopy, reveals that the region comprising the Zn-binding motif is helical and that zinc binding is likely to be histidine mediated.

EXPERIMENTAL PROCEDURES

Histatin Synthesis and Purification. Histatin was synthesized on a Synergy Peptide Synthesizer model 432A (Applied Biosystems), which performs solid-phase synthesis with fluorenyl-9-methoxycarbonyl derivatives (*15*−*17*). Cleavage from the resin was achieved with a mixture of trifluoroacetic acid and ion scavengers.The peptide was separated from resin and precipitated from the cleavage mixture with methyl *tert*-butyl ether. The crude peptide was dissolved and lyophilized for storage.The peptide was purified on a Beckman HPLC apparatus with an Aquapore RP-300 reversed-phase preparative column and a gradient of 0−60% (v/v) acetonitrile containing 0.2% trifluoroacetic acid. The eluate was monitored by absorbance at 220 nm. The elution time of the synthesized histatin-5 was the same as the histatin purified from whole saliva. Purified peptide was freeze-dried and stored at − 80 °C. Automated Edman degradation was performed with an Applied Biosystems Model 473A pulsed-liquid sequencer with on-line detection of phenylthiohydantoin amino acids.

Preparation of Liposomes. Small unilamellar liposome sonicated vesicles made with EYPC and EYPA and having an average diameter of 30−40 nm were made by the method of Huang (*18*). Phospholipids, dissolved in chloroform,were dried under a N_2 flow. Buffer (50 mM Tris/HCl, pH 7.2) was then added to the thin film of lipids, and after hydration at room temperature, the suspension was vigorously vortexed. The multilamellar vesicles obtained were sonicated in a Branson bath sonicator for 20 min, above their transition temeperature (*19*).

Aggregation Assay. Liposome aggregation was monitored using 90° light scattering with an Aminco Bowman fluorescence spectrometer. Excitation and emission were both set at 400 nm. The initial scattering from the liposomes was set to zero, and the change in scattering intensity upon histatin-5 addition was monitored as a function of time. As described by Kerker (*20*) for particles that are small compared with the wavelength of light, the relative increase of scattered light due to aggregation will be equal to the mass average aggregate size.

Fusion Assay. Membrane lipid intermixing was estimated by the method based on RET as described by Struck et al. (*21*). NBD-PE and Rho-PE were used as donor and acceptor fluorescent lipids. Briefly, two populations of SUVs were made as described above, containing 50 μM total lipid: one was labeled with 2% (mol/mol) Rho-PE, and the other was labeled with 1% NBD-PE. Fusion was induced by adding aliquots of peptide (1.5−7 μM) to a vesicle suspension (0.750 mL of each population, 50 μM total phosphorus) directly in the cuvette used for fluorescence determination, at 37 °C. The excitation wavelength was set at 475 nm, and emission was recorded at 530 nm. The fluorescence corresponding to the maximal fusion level was determined relative to the fluorescence of a vesicle population (50 μM total phosphorus) with identical lipid composition but containing 1.5% Rho-PE and 0.5% NBD-PE. Fluorescence experiments were performed with an Aminco Bowman fluorescence spectrometer, equipped with a jacketted cuvette.

Circular Dichroism Spectroscopy. CD spectra were measured with a Jasco J 600 CD spectropolarimeter calibrated with camphorsulfonic acid. Spectra were recorded between 200 and 250 nm using a path length of 0.1 cm, a time constant of 1.0 s, a 2 nm bandwidth, and a scan rate of 2 nm/min. A total of 4 scans were used for each experiment. The average was correct by 4 scans of the solvent alone. A 0.1 cm sealed and thermostatically controlled quartz cell was used for all CD spectra.

Mean residue ellipticity (θ_{MRW} in deg·cm^2·dmol^{-1}) is reported. The degree of helix formation was calculated as the ratio between the mean residue ellipticity observed at 222 nm and the mean residue ellipticity expected for 100% helicity, evalued by using the equation for the chain-length dependence of helices (*22*):

$$[\theta]_{222} = (f_H - ikN)[\theta]_{H\lambda}^{\infty}$$

where $[\theta]_{H\lambda}^{\infty}$ is the max mean residue ellipticity of a helix of infinite length (−39 500 deg·cm^2·dmol^{-1} at 222 nm) (*23*), f_H is the fraction of helix in the molecule, i is the number of possible helical segments, N is the number of residues, and k is a wavelength-dependent constant (2.57 at 222 nm). Thus, in the peptide used in our study, of chain length 24 residues and with an f_H of 0.83, the expected value of the mean residue ellipticity for 100% helicity was −28 555 deg·cm^2·dmol^{-1}. The samples for circular dichroism experiments in TFE were prepared at concentrations of 50 and 150 μM histatin-5.

The spectra in the presence of cations were collected at concentrations of 5, 10, 50, and 100 μM $ZnCl_2$, $CaCl_2$, and $CuCl_2$ both in 50 mM Tris-HCl buffer and in the presence of unilamellar liposomes (with a 1:15 peptide:lipid ratio).

Nuclear Magnetic Resonance Spectroscopy. NMR studies samples were prepared at a concentration of 10 mM in 90% deuterated 2,2,2-trifluoroethanol (Reidel-de-Haen) and 10% 0.1 M KCl solution. NMR spectra of histatin-5 (pH 3.6) were run at 25 °C on a Bruker AM 400 instrument operating at 400.13 MHz. Two-dimensional NMR experiments were performed in the phase-sensitive mode using TPPI (*24*) for quadrature detection in the indirect dimension. A total of 512 increments were collected. The number of scans was optimized in order to obtain a satisfactory signal-to-noise ratio. TOCSY experiments were performed using a MLEV-17 spinlock composite pulse sequence (*25*, *26*) with a typical mixing time of either 30 or 70 ms in order to observe either direct or remote connectivities. NOE dipolar-correlated two-

[1] Abbreviations: CD, circular dichroism; DMSO, dimethyl sulfoxide; EYPC, egg yolk phosphatidylcholine; EYPA, egg yolk phosphatidic acid; HPLC, high-pressure liquid chromatography; NBD-PE, 7-nitro-2,1,3-benzoxadiazolephosphoethanolamine; NOESY, nuclear Overhauser enhancement spectroscopy; RET, resonance energy transfer; Rho-PE, tetramethylrhodamine-phosphoethanolamine; RMSD, root-mean-square deviation; NOE, nuclear Overhauser effect; SUVs, small unilamellar vesicles; TFE, trifluoroethanol; TOCSY, total correlation spectroscopy; TPPI, time proportional phase increment.

Table 1: Amino Acid Sequences of Salivary Histatins[a]

Histatin 1:	DS^{p}HEKRHHGYRRKFHEKHHSHREFPFYGDYGSNYLYDN
Histatin 2:	RKFHEKHHSHREFPFYGDYGSNYLYDN
Histatin 3:	DSHAKRHHGYKRKFHEKHHSHRGYRSNYLYDN
Histatin 4:	RKFHEKHHSHRGYRSNYLYDN
Histatin 5:	DSHAKRHHGYKRKFHEKHHSHRGY
Histatin 6:	DSHAKRHHGYKRKFHEKHHSHRGYR
Histatin 7:	RKFHEKHHSHRGY
Histatin 8:	KFHEKHHSHRGY
Histatin 9:	RKFHEKHHSHRGYR
Histatin 10:	KFHEKHHSHRGYR
Histatin 11:	KRHHGYKR
Histatin 12:	KRHHGYK

[a] S^{p} represents a phosphoserine residue.

dimensional spectra were obtained using NOESY (*27*). The mixing times were 120, 240, and 320 ms. Data were processed on a microVax II with the "TRITON" two-dimensional NMR software written by Boelens and Vuister of the University of Utrecht, The Netherlands (courtesy of Prof. R. Kaptein). FIDs were multiplied by a $\pi/3$ shifted sinebell apodization function in both dimensions.

In all homonuclear two-dimensional experiments, a 1024 $\times$ 1024 matrix in the phase-sensitive mode was thus obtained with a digital resolution of about 5 Hz/point. Base line correction was carried out in both dimensions using a fifth-order polynomial fit routine present in the same program.

Structure Calculation from NMR Data. Structure calculations were performed with the program X-PLOR using a simulated annealing protocol (*28*). Interproton distance constraints were derived from the NOESY spectra. NOEs were translated into upper limited distance constraints by visual inspection of their intensities, using the following qualitative criteria: strong NOEs were set to distances lower than 0.3 nm; medium, lower than 0.4 nm; and weak, lower than 0.5 nm. Pseudoatoms were added to interproton distance restraints where necessary. A fully extended starting structure was generated and subjected to 1800 steps of molecular dynamics at 1000 K followed by 9000 cooling steps to 100 K. A 5 fs time step was used. Finally, 1000 steps of Powell energy minimization were performed. Using this method, 50 structures were generated. All 50 structures were refined through 12 000 cooling steps from 1000 K followed by 5000 steps of Powell energy minimization. Finally, structures with NOE restraint violations greater than 0.5 Å were discarded.

RESULTS

Histatin Sequence Analysis. The primary structures of several histatins are reported in Table 1. The amino acid composition of histatin-5 is rather polar with an elevated number of basic residues distributed over the entire length of the polypeptide chain. In particular, seven histidins, four lysines, and three arginines confer a net positive charge of +5 at physiological pH. On the contrary, a limited number of hydrophobic residues are present in the primary structure. This amino acid composition does not confer an amphiphilic character to the molecule.

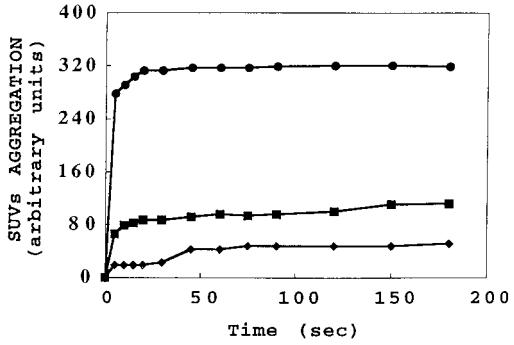

FIGURE 1: Time course of histatin-5-induced SUV aggregation monitored by the change of 90° light scattering as described under Experimental Procedures. The change in scattering intensity of samples was monitored at different histatin-5 concentrations: 4 μM (◆); 7 μM (■); and 14 μM (●).

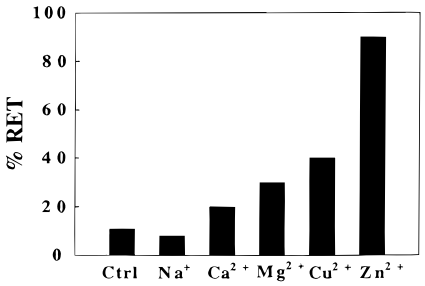

FIGURE 2: Effect of different cations on the ability of histatin-5 to induce SUV fusion. Fusion was started by the addition of 7 μM histatin-5 (Ctr), in the presence of 100 mM NaCl (Na^+) or 1 mM $CaCl_2$ (Ca^{2+}) or 1 mM $MgCl_2$ (Mg^{2+}) or 600 μM $CuCl_2$ (Cu^{2+}) or 10 μM $ZnCl_2$ (Zn^{2+}). % RET was detected after 15 min incubation of liposomes as described under Experimental Procedures. In the absence of histatin-5, the indicate concentrations of these ions induced less than 5% liposome fusion in 15 min.

Aggregation Assay. Aggregation of liposomal membranes was monitored by observing changes in the light scattering at 400 nm at different EYPA concentrations. The maximum degree of aggregation was obtained with 20% EYPA in the presence of histatin-5 at a 14 μM concentration. As shown in Figure 1, the aggregation effect is obtained immediately after the addition of the peptide. After the initial effect, the aggregation state remained constant.

Fusion Assay. Fusion of liposomal membranes was monitored by observing changes in the RET between fluorescent lipid probes when histatin-5 was added to vesicle solutions. In the presence of SUVs with 20% (mol/mol) phosphatidic acid (EYPC/EYPA 8:2), histatin-5 has a very low fusogenic ability, but when Zn^{2+} ions were added nearly complete fusion was observed (Figure 2). On the basis of these results and to probe the selectivity of zinc to induce membrane fusion, different cations (Ca^{2+}, Cu^{2+}, Mg^{2+}, Na^+) were examined. Our results clearly show that zinc ions selectively induce fusogenic activity of histatin-5. In fact, at a Zn^{2+} concentration of 10 μM, the fusion activity linearly increases with the peptide concentration, reaching a maximum value of RET at a concentration of 7 μM histatin-5 (Figure 3A). Figure 3B shows a typical time course of liposome fusion induced by 7 μM histatin-5, monitored by RET. In the concentration range of histatin tested (1.5−7 μM), the fusion between liposomes occurred within the first 30 s (with our experimental system it was impossible to follow faster events). After the initial burst, the RET

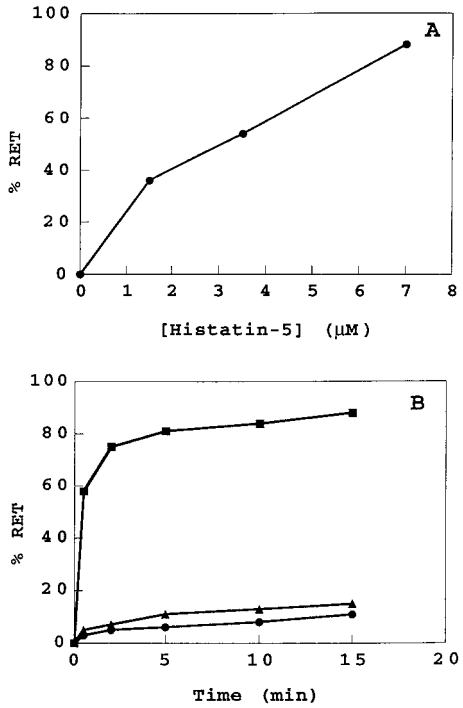

FIGURE 3: Histatin-5 induces liposome fusion in the presence of $ZnCl_2$. (A) Rate of fusion of EYPC/EYPA (80:20) liposomes as a function of histatin-5 concentration, assayed by RET as described in Figure 2. Fusion between vescicles was started by the addition of 10 μM $ZnCl_2$ and histatin-5. The RET values were determined after 15 min. (B) Time course of histatin-5-induced liposome fusion monitored by RET at 37 °C in the same conditions as in Figure 2. The fluorescence of samples containing 7 μM histatin-5 (●), 10 μM $ZnCl_2$ (▲), or 7 μM histatin-5 plus 10 μM $ZnCl_2$ (■) was monitored at different times as described under Experimental Procedures.

remained constant, indicating that (a) the effect was nearly instantaneous and (b) the histatin redistribution after binding to the membrane is a very improbable event, since this would gradually cause fusion of the whole liposome population. Under the same experimental conditions, neither histatin-5, in a range of concentration (1.5−7 μM) in the absence of Zn^{2+} ions, nor 10 μM Zn^{2+} ions alone was able to induce liposome fusion.

CD Spectroscopy. The circular dichroism spectra of histatin-5 in water solution or in water/2,2,2-trifluoroethanol mixtures are reported in Figure 4. The dichroic profile indicates that the peptide assumes a random coil conformation in water. Increasing the concentration of TFE caused a substantial increase in negative ellipticity at 208 nm ($\pi \rightarrow \pi^*$ transition) and at 222 nm ($n \rightarrow \pi^*$ transition), indicating the formation of an α-helix. A gradual increase of the helix content was observed with increasing TFE concentration. At 90% TFE v/v, the mean residue ellipticity was −5420 deg·cm²·dmol⁻¹, which allowed us to evaluate a degree of helix corresponding approximately to 20% of the length of the peptide chain. The mean residue ellipticity observed was independent of the peptide concentration; in fact, the CD signals at 150 μM histatin-5 in TFE were like that obtained at 50 μM, indicating that the peptide was essentially monomeric.

The effects on CD spectra of the presence of SUVs were investigated in order to reveal the ability of these membrane models to induce conformational changes on histatin-5. In

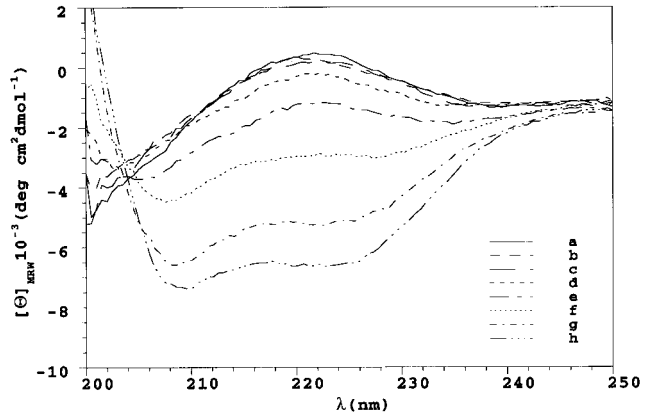

FIGURE 4: Circular dichroism spectra of histatin-5 as a function of TFE concentration. The experimental conditions are reported under Experimental Procedures. (a) 50 μM histatin-5 in water at pH 3.6; (b) 10% TFE; (c) 20% TFE; (d) 40% TFE; (e) 60% TFE; (f) 80% TFE; (g) 90% TFE; and (h) 100% TFE.

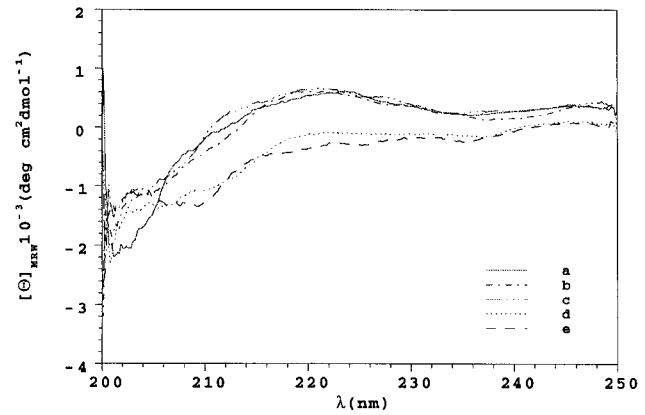

FIGURE 5: CD spectra of histatin-5 as a function of Zn^{2+} concentration, in 50 mM Tris-HCl, pH 7.3, with 750 μM EYPC/EYPA (8:2): (a) 50 μM histatin-5; (b) histatin-5 with 5 μM $ZnCl_2$; (c) with 10 μM $ZnCl_2$; (d) with 50 μM $ZnCl_2$; (e) with 100 μM $ZnCl_2$.

the presence of liposomes, with or without phosphatidic acid, at a 1:15 molar ratio, a very slight tendency to produce a CD profile which is characteristic of helical conformation is seen. Addition of divalent cations (Zn^{2+}, Ca^{2+}, and Cu^{2+}) in the presence of liposomes, with neutral and charged phospholipids, was also investigated in order to reveal the effects of these cations on the conformation of this peptide.

As shown in Figure 5 the addition of zinc to the complex of histatin-5 and SUVs, obtained from negatively charged phospholipids, induces changes in the CD profile characteristic of a helical conformational change, characterized by the appearance of two minima at 208 and 222 nm. The effect observed is specifically induced by Zn^{2+} cations. In fact, the equimolar addition of other divalent cations such as Ca^{2+} and Cu^{2+} did not produce similar changes in the CD spectrum (data not shown). Moreover, the CD experiments indicate that in the presence of zinc and liposomes from neutral phospholipids the CD profile of histatin-5 does not change with respect to that obtained in the absence of zinc.

NMR Spectroscopy. The two-dimensional NMR experiments were carried out both in water and in a mixed solvent at the minimum TFE:water ratio where a defined structure was observed on the basis of the CD results. In the water/TFE mixture, a marked increase of the dispersion of

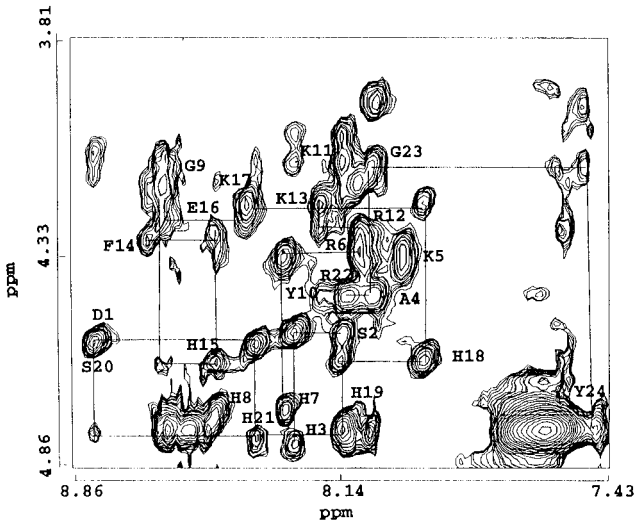

FIGURE 6: Fingerprint region (NH−CHα) of the NOESY spectrum of histatin-5 in TFE solution at 25 °C. The αN (*i*; *i*+1) connectivities are labeled.

resonances was observed in the NMR spectrum, clearly indicating the presence of different magnetic environments typical of secondary structure.

Analysis of two-dimensional NMR spectra led to the complete assignment of the resonances of the spin systems. This result was achieved by TOCSY experiments at different isotropic mixing times to reveal direct and remote connectivities. The spin systems of the NH resonances were observed with few interferences and overlaps.

The analysis of the NOESY spectrum of histatin-5 led to the sequence-specific assignment of the peptide, from residue 1 to residue 24, following the through-space dipolar connectivity (NOE) of protons between sequential residues. The αN (*i*; *i*+1) sequential assignments were obtained following the dipolar connectivities observed at different mixing times as reported under Experimental Procedures. The aromatic residues comprising seven histidines, one phenylalanine, and two tyrosines were completely assigned following both the scalar connectivities and the NOEs between protons of rings and *β* protons of the side chain. As a starting point, the connectivity between the CHα of Glu-16 and the NH of Lys-17 was chosen. In fact, Glu-16 is unique in the sequence and well recognizable as a spin system in the TOCSY spectrum from its chemical shift values. Many parts of the sequential assignment were confirmed by observing *β*N (*i*; *i*+1) connectivities.

In the fingerprint region, the spectral dispersion of the NH resonances is rather narrow with respect to that usually observed for highly structured proteins. This indicates that histatin-5 has a limited extent of secondary structure. This spectral region, which contains NOE connectivities between CHα and NH resonances, is shown in Figure 6 together with the indication of some steps for sequential assignments. The complete assignment of the resonances contained in the NMR spectrum as well as those due to aliphatic protons is reported in Table 2.

Results leading to the solution structure of histatin-5 in a water/TFE mixture are summarized in Figure 7. In this scheme, the NOE contacts observed are reported together with an estimation of the relative intensities.

Table 2: ^{1}H Chemical Shifts (ppm) of Salivary Histatin-5 in 90% TFE at 25 °C, pH 3.6[a]

residue	NH	Hα	Hβs	Hγs	Hδs	others
Asp1	8.79	4.55				
Ser2	8.14	4.52	4.07; 4.0			
His3	8.27	4.81	3.29; 3.44		7.36	8.50
Ala4	8.08	4.34	1.56			
Lys5	7.99	4.30	2.0; 1.85		1.67	ϵ3.14
Arg6	8.09	4.32	2.0; 1.98		3.3	ϵ7.28
His7	8.30	4.72	3.47; 3.38		7.41	8.54
His8	8.47	4.73	3.47		7.48	8.60
Gly9	8.61	4.12; 4.06				
Tyr10	8.21	4.43	3.23		7.17	
Lys11	8.10	4.13	1.86; 2.02	1.68; 1.56	1.86	ηN7.80 ϵ3.12
Arg12	8.11	4.26	2.05	1.87; 1.78	3.35	
Lys13	8.20	4.18	2.03	1.56	1.67	ϵ3.09
Phe14	8.65	4.27	3.23; 3.13		7.17	7.28; 6.89
His15	8.48	4.56	3.57		7.57	8.63
Glu16	8.62	4.23	2.40; 2.32	2.78; 2.63		
Lys17	8.39	4.18	2.03	1.57; 1.47	1.77	ϵ3.02
His18	7.92	4.58	3.32; 2.99		7.06	8.07
His19	8.14	4.77	3.45; 3.32		7.41	8.58
Ser20	8.80	4.54	4.09; 4.04			
His21	8.37	4.79	3.44		7.47	8.60
Arg22	8.14	4.43	1.95; 1.88	1.73	3.27	ϵ7.12
Gly23	8.05	4.08; 3.91				
Tyr24	7.50	4.75	3.21; 3.09		7.17	6.89

[a] Chemical shifts were determined ±0.02 ppm relative to the proton resonance of H_2O at 4.8 ppm.

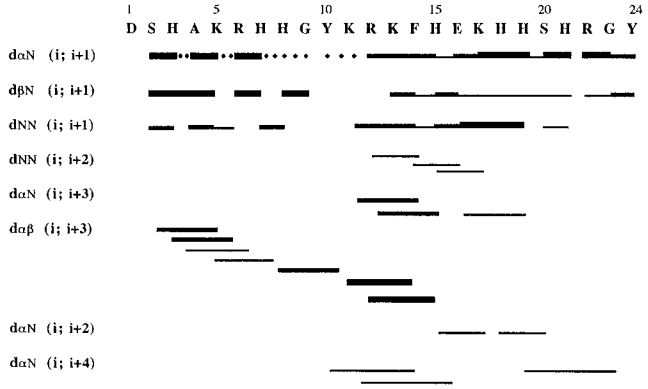

FIGURE 7: Summary of NOE connectivities found in the NOESY spectra of histatin-5 in TFE solution together with related intensities and elements of secondary structure found. The thickness of the bars indicates the NOE is strong, medium, and weak, respectively.

The (*i*; *i*+3) connectivities are usually considered diagnostic for the presence of an α-helix conformation (*29*). In our case, the *αβ* (*i*; *i*+3) contacts indicate such a helical conformation from Ser-2 to Gly-9 and from Lys-11 to His-15, while in the region 16−19 the large number of NOEs indicates a narrower helicoidal radius and a closer conformational folding than in an α-helix conformation. The absence of αN (*i*; *i*+3) and (*i*; *i*+4) NOE contacts in the region 2−9 may be accounted for either by the weakening of the NOE, due to local conformational mobility, or by the chemical exchange of NH protons due to a higher exposure to the solvent. Also, contacts between aromatic side chain protons and protons of other residues have been observed in the NOESY, for example, between the ring protons of Tyr-10 and CHα of Gly-9. Attempts to read with some accuracy the $^3J_{HNH\alpha}$ coupling constants failed, due to resonance broadening induced by solvent viscosity.

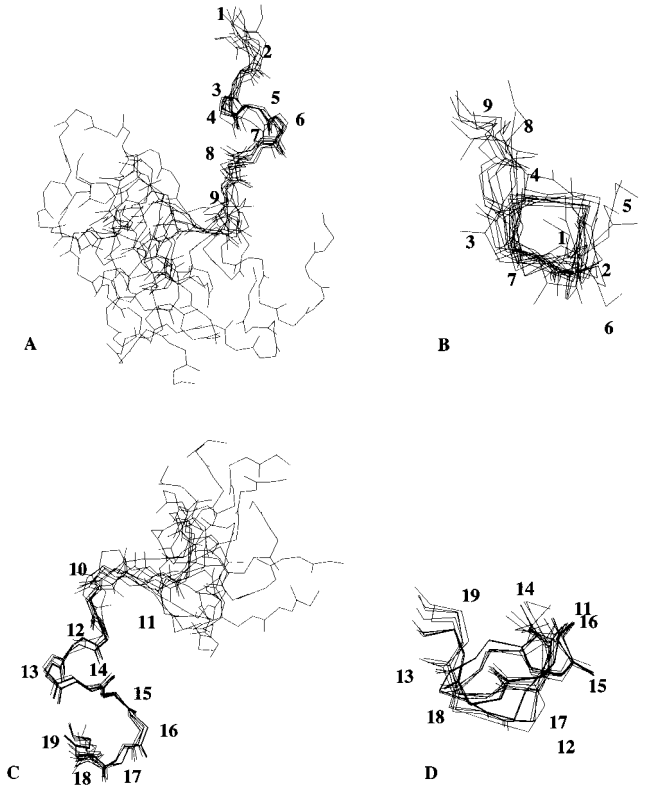

FIGURE 8: Superposition of converged backbone conformations of histatin-5 (RMSD ≤1 Å), deduced from restrained molecular simulation studies, using NOE data. Family of 8 conformations superimposed from residues 2 to 9 of histatin-5 is reported in (A) and (B) (edge view and top view, respectively); family of 10 conformations superimposed from residue 10 to residue 19 is reported in (C) and (D) (edge view and top view, respectively).

The final structure calculations involved 146 NOE distance restraints, of which 46 were sequential and 18 were medium-range (less than *i*; *i*+5). No hydrogen bond restraints were included in the structure calculation. Distance geometry and subsequent refinement by molecular dynamics were performed following the procedure reported under Experimental Procedures. The results indicated that, under the experimental conditions employed, histatin-5 has internal mobility between Gly-9 and Lys-11. For this reason, the N-terminal and C-terminal regions of the molecule have been treated separately. The two structures obtained are reported in Figure 8.

DISCUSSION

A complete understanding of the structure−function relationships of active peptides has remained elusive owing to the intrinsic flexibility of small peptides and the large number of conformations that can exist for linear peptides in solution. There is now good experimental evidence that short linear peptides and protein fragments can assume organized local structures in mixed solvent systems with dual lipophilic and aqueous nature such as TFE/water mixtures (*30, 31*). The molecular characterization of these local structures could be of fundamental importance in understanding the mechanism of action of numerous antimicrobial peptides secreted into the biological fluids.

In the current study, we have focused our attention on the sequence motif HEXXH present in the antimicrobial salivary peptide histatin-5, and conserved in all major human histatins, within the presumed C-terminal functional domain. This sequence has not been recognized in any other antimicrobial peptide so far characterized and highlights the novelty of histatins as antimicrobial agents.

This short sequence is a recognized zinc-binding motif present in numerous proteins including adamalysins, metrixins, collagenasis, tetanus toxin, and others (*32*). Our experiments clearly demonstrate that the ability of histatin-5 to fuse SUVs with negatively charged phospolipids is selectively induced by the presence of Zn^{2+} ions. The ability of this peptide to interact with the metal, as reported above, may be due to the presence of the specific motif. We have analyzed the secondary structure of histatin-5 in TFE/water solution, by NMR spectroscopy, so as to determine the conformation of the hypothetical zinc-binding motif in a membrane-like environment. The solvent-induced secondary structure led us to the identification of two helical tracts, one from residue Ser-2 to residue Gly-9 and the other from His-11 to His-19. The C-terminus of the second helical tract is less well-defined than the tract N-terminus. In fact, from Glu-16 to His-19, strong NN (*i*; *i*+1) contacts and few αN (*i*; *i*+2) and αN (*i*; *i*+3) contacts can be observed. There is an absence of αβ (*i*; *i*+3) and αN (*i*; *i*+4) contacts. We have performed a comparison between our structure and the structure determined in DMSO by Raj et al. (*33*). In the latter case, the peptide appears completely unstructured in H_2O/D_2O solution while it is completely helical structured in DMSO. Following Sykes (*34*), we have calculated the ratio between the chemical shift of CHα protons of the more structured form to the less structured one (DMSO/TFE/H_2O).The results obtained indicate that the ratio between the chemical shift of the CHα resonances is parallel with the exception of three residues. The CHα residues of Gly-9 and His-19 are shifted upfield while that of Lys-11 is more downfield shifted in DMSO than in TFE/water. This clearly confirms the findings obtained from our NMR data indicating a break in the histatin-5 secondary structure between residues Gly-9 and Lys −11. This result is also in agreement with the helix-breaking character of the Gly residue.

The higher mobility found in our peptide structure with respect to that determined in DMSO can be explained considering the lipophilic and aqueous nature of our system (TFE/water). In fact, an increase of helix content was observed in CD spectra, when histatin-5 was solubized in 100% TFE (Figure 4).

Moreover, our CD results clearly indicate that in the presence of negatively charged membranes, the C-terminal region of the histatin, containing the zinc-binding motif, undergoes secondary structure stabilization when zinc ions are added. This result is similar to that obtained by Huang et al. (*35*), who studied the interactions of the Aβ1−40 amyloid peptide with zinc ions and found that solvents able to promote α-helical conformations favor peptide−zinc interactions. NMR experiments are in progress to better characterize the conformational change that histatin-5 undergoes in the presence of zinc ions, in a membrane-like environment.

The importance of the histidine residues present in the presumed functional domain of histatin-5, to retain its antimicrobial activity, has been recently demonstrated by mutagenesis experiments (*36*). In this work, Driscoll et al. expressed a variant histatin in which all the histidines, at

positions 15, 18, 19, and 21, were converted to glycines and determined that this mutant peptide was less effective in killing *C. albicans* blasticonidia compared to the native histatin-5. Furthermore, Zhuo et al. (*37*) have demonstrated that duplication of the functional domain with recombinant histatin-3 enhanced candidacidal activity. Proposed mechanisms of action of the antimicrobial peptides have considered the ability of these molecules to interact with the membrane of the pathogen microorganisms. The peptide−membrane interaction has been correlated to the amphipathic character and to the ability of the peptides to assume an α-helical secondary structure in solution, thereby altering the membrane permeability by forming channels (*38*). Histatin-5, unlike other naturally occurring antimicrobial polypeptides, such as magainins and defensins, does not adopt amphiphilic structure, precluding its insertion into microbial membranes and formation of ion channels across membranes. It seems likely that electrostatic forces may play a major role in the aggregation and fusion of negatively charged vesicles by histatin.

Decreased aggregation was, in fact, observed when histatin was mixed with neutral SUVs, indicating that the absence of charge−charge interactions greatly reduces the ability of this peptide to aggregate lipid vesicles. This suggests that the positively charged histatins might play a role in destabilizing the negatively charged lipid vesicles by reducing the electrostatic repulsive forces between the individual lipids and the opposing bilayer. This behavior is reminiscent of that of other cationic antimicrobial peptides such as melittin and defensins which exert their action primarily on negatively charged lipid vesicles. The ability of histatin to destabilize and fuse negatively charged membranes appears strictly dependent on the presence of zinc ions. The action of zinc seems to be extremely selective in comparison to the action of other divalent cations and can be correlated with histatin-5 conformational changes, seen by CD spectroscopy (see Figure 5). This conformational change occurs only in the presence of negatively charged vesicles and does not occur in the presence of neutral phospholipids. Recently, a speculative model has been proposed to explain the fusogenic activity of the antimicrobial defensins, essentially based on the dimeric structure of these peptides (*39*).

Our preliminary experiments, performed with histatin-5 in a hydrophobic environment, demonstrate that zinc ions induce peptide dimerization (manuscript in preparation), thus supporting the fusogenic activity of histatin-5. It appears, therefore, that the antimicrobial action of histatin-5 could be explained by considering two specific molecular interactions with phospholipid membranes: the first, in which the peptide promotes, by charge interactions, the aggregation of the membranes; and the second in which the structural stabilization of the functional domain induced by zinc ions favors peptide dimerization and destabilization of the lipid bilayer promoting membrane fusion. It is interesting to note that the charged and functional domains of histatin-5 are localized in two distinct regions of the molecule, with charged residues localized in the N-terminal half, whereas the functional domain, which promotes the interaction with zinc and dimerization, is confined in the C-terminal region. This hypothesis is in agreement with the result of Raj et al. (*10*), who demonstrated that a synthetic 16-residue C-terminal fragment of histatin-5 was as active as the whole peptide itself. In fact, the loss of the first 8 amino acids does not abolish the cationic nature of the peptide.

In conclusion, the peculiar structural and functional characteristics of histatin-5 with respect to other antimicrobial peptides were examined in detail by several spectroscopic techniques. Our results reveal that the action of this antimicrobial peptide is likely mediated by the presence of zinc ions, although further evidence will be required to confirm and refine the precise mechanism of action.

ACKNOWLEDGMENT

Fabio Bertocchi is acknowledged for the skillfull technical assistance in the NMR experiments. We thank Dr. Beatrize F. de Arcuri for fluorescence experiments.

REFERENCES

1. Zasloff, M. (1992) *Curr. Opin. Immunol. 4*, 3−7.
2. Boman, H. G. (1991) *Cell 65*, 205−207.
3. Shomers, J. P., Tabak, L. A., Levine, M. J., Mandel, I. D., and Hay, D. I. (1982) *J. Dent. Res. 61*, 397−399.
4. Wong, R. S. C., Hofman, T., and Bennick, A. (1979) *J. Biol. Chem. 254*, 4800−4808.
5. Oppenheim, F. G., Yang, Y. C., Diamond, R. D., Hyslop, D., Offner, G. D.and Troxler, R. F. (1986) *J. Biol. Chem. 261*, 1177−1182.
6. Oppenheim, F. G., Xu, T., McMillian, F. M., Levitz, S. M., Diamond, R. D., Offner, G. D., and Troxler, R. F. (1988) *J. Biol. Chem. 263*, 7472−7477.
7. Troxler, R. F., Offner, G. D., Xu, T., Vanderspek, J. C., and Oppebheim, F. G. (1990) *J. Dent. Res. 69*, 2−6.
8. Lal, K., Santarpia, R. P., III, Xu, L., Manssurri, F., and Pollock, J. J. (1992) *Oral Microbiol. Immunol. 7*, 44−50.
9. Oppenheim, F. G., Yang, Y. C., and Troxler R. F. (1985) *J. Dent. Res. 64*, 239.
10. Raj, P. A., Edgerton, M. E., and Levine, M. J. (1990) *J. Biol. Chem. 265*, 3898−3905.
11. Bevins, C. L., and Zasloff, M. (1990) *Annu. Rev. Biochem. 59*, 396−414.
12. Lear, J. D., Wasserman, Z. R., and Degrado, W. F. (1988) *Science 240*, 1177−1181.
13. Jongeneel, C. V., Bouvier, J., and Bairoch, A. (1989) *FEBS Lett. 242*, 211−214.
14. Xu, T., Telser, E., Troxler, R. F., and Oppenheim, F. G. (1990) *J. Dent. Res. 69*, 1717−1723.
15. Merrifield, R. B. (1963) *J. Am. Chem. Soc. 85*, 2149.
16. Merrifield, R. B., Stewart, J. M., and Jerberg, N. (1966) *Anal. Chem. 38*, 1905−1914.
17. McFerran, N. V., Walker, B., McGurk, C. D., and Scott, F. C. (1991) *Int. J. Pept. Protein Res. 37*, 382−387.
18. Huang, C. H. (1969) *Biochemistry 8*, 344−355.
19. Rufini, S., Pedersen, S. Z., Desideri, A., and Luly, P. (1990) *Biochemistry 29*, 9644−9651.
20. Kerker, M. (1969) *The scattering of light and other electromagnetic radiation*, pp 432−433, Accademic Press, New York.
21. Struck, D. K., Hoekstra, D., and Pagano, R. E. (1981) *Biochemistry 20*, 4093−4099.
22. Chen, Y. H., Yang, J. T., and Chaun, K. H. (1974) *Biochemistry 13*, 3350−3359.
23. Chang, T. C., Wu, C. S., and Yang, J. T. (1978) *Anal. Biochem. 91*, 13−31.
24. Marion, D., and Wüthrich, K. (1983) *Biochem. Biophys. Res. Commun. 113*, 967−974.
25. Braunschweiler, L., and Ernst, R. R. (1983) *J. Magn. Reson. 53*, 521−528.
26. Bax, A., and Davis, D. G. (1985) *J. Magn. Reson. 65*, 355−360.
27. Jeener, J., Meier, B. H., Bachmann, P., and Ernst, R. R. (1979) *J. Chem. Phys. 71*, 4546−4553.

28. Brunger, A. T. (1992) *X-PLOR (version 3.1) Manual*, Yale University Press, New Haven, CT.
29. Wüthrich, K. (1986) *NMR of Proteins and Nucleic Acids*, John Wiley & sons, New York.
30. Waterhous, D. V., and Johnson, W. C., Jr. (1994) *Biochemistry 33*, 2121−2128.
31. Jasanoff, A., and Fersht, A. R. (1994) *Biochemistry 33*, 2129−2135.
32. Bode, W., Gomis-Ruth, F. X., and Stöckler, W. (1993) *FEBS Lett. 331*, 134−140.
33. Raj, P. A., Marcus, E., and Sukumaran, D. K. (1998) *Biopolymers 45*, 51−67.
34. Wishart, D. S., Sykes, B. D., and Richards, F. M. (1992) *Biochemistry 31*, 1647−1651.
35. Huang, X., Atwood, C. S., Moir, R. D., Hartsborn, M. A., Vonsattle, J. P., Tanzi, R. E., and Bush, A. I. (1997) *J. Biol. Chem. 272*, 26464−26470.
36. Driscoll, J., Duan, C., Zuo, Y., Xu, T., Troxler, R., and Oppenheim, F. G. (1996) *Gene 177*, 29−34.
37. Zhuo, Y., Xu, T., Troxler, F., Li, J., Driscoll, J., and Oppenheim, F. G. (1995) *Gene 161*, 87−91.
38. Ghung, B. H., Anantharamiah, G. M., Brouilette, C. G., Nishida, T., and Segrest, J. P. (1985) *J. Biol. Chem. 260*, 10256−10262.
39. Fujii, G., Selsted, M. E., and Eisenberg, D. (1993) *Protein Sci. 2*, 1301−1312.

BI990212C